RESEARCH ARTICLE | JANUARY 10 2022

Xenon mobility in γ-uranium and uranium–molybdenum alloys

A. Rafi M. Iasir; Karl D. Hammond

Journal of Applied Physics 131, 025105 (2022)
https://doi.org/10.1063/5.0059157

Journal of Applied Physics ARTICLE scitation.org/journal/jap

Xenon mobility in γ-uranium and uranium–molybdenum alloys

Cite as: J. Appl. Phys. **131**, 025105 (2022); doi: 10.1063/5.0059157
Submitted: 6 June 2021 · Accepted: 14 December 2021 ·
Published Online: 10 January 2022

View Online Export Citation CrossMark

A. Rafi M. Iasir[1,2] and Karl D. Hammond[1,2,a)]

AFFILIATIONS

[1]Nuclear Engineering Program, University of Missouri, Columbia, Missouri 65211, USA
[2]Department of Chemical Engineering, University of Missouri, Columbia, Missouri 65211, USA

[a)]**Author to whom correspondence should be addressed:** hammondkd@missouri.edu

ABSTRACT

Diffusion in bcc uranium and U–Mo alloys is of great interest because fission gas and other fission products impact the performance of nuclear fuels. We investigate the mobility of xenon and molybdenum in bcc uranium (γ-U) and metallic U–Mo alloys by calculating the migration energies of xenon and molybdenum for various local compositions using density functional theory. We also calculate the solute–vacancy binding energies of different solutes to vacancies in bcc uranium. We find that the solute–vacancy binding energy in bcc uranium is significantly higher than it is in other bcc metals (e.g., Fe and W). We also find that the migration energy of molybdenum is substantially higher than the migration energy of xenon, indicating that xenon is much more mobile than molybdenum in bcc uranium. The presence of molybdenum in the nearest-neighbor shell around a xenon atom typically increases the migration energy of xenon, which indicates a reduction of xenon mobility in U–Mo alloys compared to pure bcc uranium.

I. INTRODUCTION

High-performance research reactors require high-enrichment uranium (HEU) fuels to attain the desired neutron flux. The replacement of HEU fuels with low-enrichment uranium (LEU) is an important antiproliferation initiative. The United States High-Performance Research Reactor (USHPRR) program is currently aiming to replace the HEU fuels currently used in high-performance reactors with LEU fuels.[1] LEU fuels require a higher uranium density than that of uranium oxides to compensate for the decrease in ^{235}U enrichment. Metallic uranium shows great promise in this regard.

Metallic fuels are usually chosen because of their high thermal conductivity and high density. Isotropic swelling behavior is desirable, but uranium, like other light actinides (Pa–Pu), has a low-symmetry crystal structure (the orthorhombic α phase) at ambient temperature and pressure, which results in anisotropic thermal and radiation-induced expansion. Pure uranium has three allotropes at atmospheric pressure: α (base-centered orthorhombic), β (tetragonal), and γ (body-centered cubic). At atmospheric pressure, α-uranium transforms to β-uranium at approximately 935 K, and β-uranium transforms to γ-uranium at approximately 1045 K.[2,3]

The γ-uranium allotrope (which is body-centered cubic) is preferred to α-uranium by nuclear engineers because it undergoes both isotropic thermal expansion and isotropic radiation-induced swelling.[4] It is not possible to retain pure γ-uranium under the required processing and radiation conditions; however, a metastable bcc phase can be obtained at room temperature by alloying with molybdenum.[5–8] A study by Kim-Ngan and Havela[9] showed that the bcc structure can also be retained at temperatures below the ordinary phase transition temperature by alloying uranium with certain metals, such as platinum, palladium, niobium, and zirconium. Molybdenum stabilizes uranium's γ phase at concentrations near the eutectoid point (11.1 wt. % Mo) and lowers the phase transition temperature from 1045 K for pure γ-uranium to 828 K for a U–Mo alloy at the eutectoid point.[10,11] Uranium alloyed with 10 wt. % molybdenum (U-10Mo, which is 21.6 at. % molybdenum) is currently being developed as a potential high-density, low-enrichment uranium fuel for high-performance research reactors.[12–14]

Uranium–molybdenum alloys have been studied extensively both experimentally[6,15,16] and theoretically.[17–21] Castellano *et al.*[22] showed that the addition of molybdenum to uranium leads to the stabilization of the γ phase using *ab initio* molecular dynamics. This thermodynamic stabilization is important because un-alloyed γ-uranium is not stable under fuel preparation and irradiation conditions.[6,8] Fission creates a variety of products, resulting in gas bubbles, metallic precipitates, and solutes in the fuel matrix. Among the many fission products, fission gas (i.e., xenon and krypton) produces some of the most significant challenges associated with nuclear fuel development. Fission gas influences the thermal conductivity, causes swelling, and impacts the neutron economy of the reactor.[23,24] The ratio of xenon to krypton in fission gases is typically nine to one.[25] The most important fission gas isotopes with short half lives are ^{133}Xe (5.25 d) and ^{135}Xe (9.1 h). In particular, ^{135}Xe has a very high neutron absorption cross section ($\sigma_a = 2.7 \times 10^6 \pm 0.1$ barns) that can lower the fuel's reactivity. Hence, the evolution of fission gases is directly related to fuel performance.

Large fission gas atoms (i.e., xenon) are mostly insoluble in the fuel matrix.[26,27] There is a significant driving force for segregation of fission gas atoms to defects, such as grain boundaries or dislocations, and consequently gas bubbles form at these sinks. Post-irradiation analysis of U–Mo alloys showed that the fission gases distribute themselves both inside the grains and along grain boundaries.[28–31] Fission gas in U–Mo alloys also forms superlattices, in which the bubbles distribute themselves in an organized array.[31–33] To understand the mechanism of the formation of gas-bubble superlattices, the rate-limiting processes involved in fission gas transport need to be studied. One of these processes is the motion of individual gas atoms through the fuel matrix, assisted by vacancies.

The behavior of fission gas has been extensively researched for common fuels, such as UO_2.[34–38] A number of theoretical approaches have also been used to understand the behavior of fission products in UO_2, including electronic structure theory.[26,27,39–45] In particular, vacancies play an important role in the diffusion of xenon because of its size relative to the metal atoms.

Solute diffusion in light actinides is a very interesting phenomenon because such solutes typically have very high diffusivities.[46–48] Diffusion of solutes in metallic uranium has not been studied extensively. However, there are some early works that provide some information about defect and impurity diffusion in uranium.[49–56] Smirnova *et al.*[57,58] studied self-diffusion in γ-uranium and U–Mo alloys using molecular dynamics. They showed that diffusion in γ-uranium, like that in other light actinides, is anomalously fast compared to bcc transition metals.

In recent years, there have been many attempts to calculate diffusion coefficients of impurities using electronic structure and atomistic methods.[59–66] Electronic structure calculations based on DFT and multi-frequency models have shown their usefulness in various works. Five-frequency models of face-centered cubic crystals[67–69] and nine-frequency (or sometimes four-frequency) models of bcc crystals[70,71] have been widely used. Methods based on electronic structure theory involve calculating the activation energies of an atom jumping to a vacancy in one of the atom's nearest-neighbor positions. This is often referred to as vacancy-mediated diffusion. The calculations employed here are based on DFT coupled with classical transition state theory (TST), which treats vibration using the harmonic oscillator approximation.[72,73]

In this study, we use DFT and TST to study the diffusion of xenon and molybdenum in γ-uranium alloys, such as U-7Mo and U-10Mo, by varying the local molybdenum concentration around the diffusing solute atom. We find that the migration energy of molybdenum is much higher than that of xenon in γ-U alloys and that the presence of molybdenum in the local environment of a xenon atom tends to decrease the mobility of xenon in γ-uranium alloys. We also calculate the vacancy–solute binding energies of several solutes in γ-uranium and find that such binding energies are generally higher in γ-uranium than in iron or aluminum.

II. THEORY

Diffusion coefficients in crystalline solids are often described by an Arrhenius equation over a wide range of temperatures. This model consists of two parameters, the migration energy, E_m, and the pre-exponential factor, D_0, with the diffusion coefficient given by

$$D = D_0 e^{-E_m/k_B T}, \tag{1}$$

where k_B is the Boltzmann constant and T is the absolute temperature. If D_0 is independent of temperature, an Arrhenius plot (D against $1/T$) gives a straight line; if D_0 changes with T, it yields a curve that falls away from the constant-D_0 line at high temperature (the left of the plot).

The migration energy is the activation energy for an atom to jump onto a nearby vacancy. According to classical transition state theory (TST), the rate at which a vacancy exchanges its place with a neighboring atom can be expressed by the Eyring–Polanyi equation,[73–75]

$$\begin{aligned} \nu = \nu^{\ddagger} \exp\left(\frac{-\Delta G_m}{k_B T}\right) &\approx \frac{k_B T}{h}\frac{Q_{\mathrm{TS}}}{Q_{\mathrm{IS}}} \exp\left(\frac{-E_m}{k_B T}\right) \\ &\approx \frac{k_B T}{h} \exp\left(\frac{-E_m}{k_B T}\right), \end{aligned} \tag{2}$$

where Q_{IS} is the vibrational partition function of the initial state and Q_{TS} is the vibrational partition function of the transition state with the vibrational mode along the minimum-energy pathway removed. In the current work, we did not calculate the jump frequencies, which are part of the Q_i terms; we instead make the approximation that the vibrational partition functions not associated with the minimum-energy pathway are unity (i.e., $Q_{\mathrm{TS}}/Q_{\mathrm{IS}} \approx 1$). In situations in which all jumps have approximately the same activation energy, as is the case with self-diffusion, the diffusion coefficient is proportional to the rate of a jump: $D = \nu\lambda^2/6$, where $\lambda = a/\sqrt{8}$ for bcc lattices[76] and a is the lattice parameter. In situations in which multiple solutes are present, such as in this work, Eq. (2) gives an estimate of the rate of each individual jump, but the net diffusion process is more complicated.

The process of diffusion in solids typically occurs by a series of jumps, each with a rate given (approximately) by Eq. (2) with different migration energies and/or pre-exponential factors, chained together. The net process of xenon diffusion will thus be linked to the process of self-diffusion (i.e., uranium diffusion), as well as the diffusion of solute atoms, such as molybdenum. The formation of multiple vacancies, which we discount here, would also have drastic effects on the rate of net xenon transport—it should be noted that both divacancies and vacancies paired with substitutional xenon are known to be bound in γ-uranium and U–Mo alloys.[77] The effective diffusion coefficient in Eq. (1) is thus a composite of several steps, and the effective diffusion coefficient and migration energy are a composite of the individual steps, weighted by their respective likelihoods of being encountered.

Metals that undergo irradiation have point defects, such as self-vacancies and self-interstitials, in the lattice. The diffusion of these defects results in microstructural changes that can impact the mechanical properties. The diffusion of vacancies is of significant interest because they form voids, dislocation loops, and clusters, and they facilitate the diffusion of substitutional solute atoms. This method of solute diffusion is controlled by the interaction between a vacancy and a solute atom. The diffusion of vacancies is particularly influenced by the presence of nearby substitutional solute atoms. Sometimes the vacancy and the solute can coexist as an atom–vacancy complex. Hence, understanding solute–vacancy interactions is an important step in developing models of diffusion in irradiated materials.[78,79] The authors are not aware of any previous results regarding solute–vacancy binding in γ-uranium for any solutes; therefore, we calculated them as part of this work.

We used defects in supercells to calculate the binding energies of solute–vacancy ($X-\square$) pairs. The binding energy is the difference between the energy at infinite separation and the energy at nearest-neighbor separation. We used the following expression to calculate the binding energy of a solute to a vacancy:

$$E_b^{X-\square} = E_{\mathrm{U}_{N-1}}^{X_1} + E_{\mathrm{U}_{N-1}}^{\square_1} - E_{\mathrm{U}_{N-2}}^{X_1\square_1} - E_{\mathrm{U}_N}. \tag{3}$$

For a bcc supercell with N sites, the cell may contain no defects (energy E_{U_N}) or it may contain a vacancy (energy $E_{\mathrm{U}_{N-1}}^{\square_1}$), a solute impurity ($E_{\mathrm{U}_{N-1}}^{X_1}$), or a solute–vacancy pair ($E_{\mathrm{U}_{N-2}}^{X_1\square_1}$). A positive binding energy means that the complex is bound. Equation (3) can also be conveniently written as the energy required to form a vacancy next to a solute (X) atom. The vacancy formation energy is

$$E_f^{\square} = E_{\mathrm{U}_{N-1}}^{\square_1} - \frac{N-1}{N} E_{\mathrm{U}_N}, \tag{4}$$

where E_{U_N} is the energy of a supercell with N uranium atoms. A positive formation energy indicates that energy must be added to form the vacancy.

The disordered nature of U–Mo alloys creates some challenges for electronic structure studies. The manner in which molybdenum is distributed among the lattice sites produces different diffusion pathways for xenon, and there are several ways to arrange molybdenum atoms on the lattice sites around a particular xenon atom. We use a combinatorial approach to estimate the probabilities (Table I) of having various numbers of molybdenum atoms in the first-nearest-neighbor shell of the bcc structure around a xenon atom. Assuming that the molybdenum atoms are arranged randomly, the probability ($\mathcal{P}$) of a particular U/Mo combination on the sites near a xenon atom can be calculated using a binomial distribution,

TABLE I. Probability of having different numbers of molybdenum atoms in the nearest-neighbor (NN) location for a bcc uranium–molybdenum alloy. We have used Eq. (5) to calculate the probabilities.

No. of Mo	U-10Mo ($x_{\mathrm{Mo}} = 0.216$)	U-7Mo ($x_{\mathrm{Mo}} = 0.157$)
0	0.182	0.302
1	0.351	0.394
2	0.290	0.221
3	0.133	0.069
4	0.037	0.013
5	0.006	0.001
6	0.0006	8.95×10^{-5}
7	2.19×10^{-5}	2.39×10^{-6}

$$\mathcal{P} = nkx_{\mathrm{Mo}}^k (1 - x_{\mathrm{Mo}})^{n-k}, \tag{5}$$

where n is the number of available nearest-neighbor positions not occupied by the vacancy (for bcc, $n = 7$), k is the number of molybdenum atoms in the nearest-neighbor shell, and x_{Mo} is the (overall) mole fraction of molybdenum. According to Table I, the probability ($\mathcal{P}$) of having more than three molybdenum atoms in the first nearest-neighbor shell is low ($< 5\%$). We assume, for simplicity, that $x_{\mathrm{Xe}} \approx 0$, meaning that these results apply in the limit of infinitely dilute xenon. This assumption allows us to ignore configurations in which two xenon atoms are near each other—this is reasonable, as such configurations would be likely to form relatively immobile bubbles as soon as they occurred.

III. METHODOLOGY

All calculations used the QuantumESPRESSO[80] simulation package with the projector augmented wave (PAW) method.[81] A full description of the uranium pseudopotential can be found in our earlier work.[82] For the elements Mo, Xe, Fe, Co, Au, Nb, and Zr, we used PAW-based pseudopotentials from the QuantumESPRESSO PS Library.[83,84] We used the exchange–correlation functional of Perdew, Burke, and Ernzerhof (PBE)[85,86] for all calculations.

DFT calculates the ground state properties of a system; however, γ-uranium is mechanically unstable at low temperatures, which results in negative shear moduli.[87] Other elements (e.g., Ti, Zr, Pr, and Hf) also have high-temperature bcc structures that are unstable at low temperature.[88,89] It is consequently challenging to study γ-uranium with DFT, particularly using a supercell that includes vacancies or defects. To perform our calculations, we used the so-called shell method,[90] in which the outer layer of atoms is fixed at crystallographic coordinates and the rest of the atoms are allowed to move freely. We used a $3 \times 3 \times 3$ supercell of bcc uranium, which consists of 54 atoms in the absence of heteroatoms or vacancies. A convergence test showed that a Monkhorst–Pack k-point mesh of $5 \times 5 \times 5$ is suitable to yield formation and migration energies that are converged to within 0.01 eV/Å.

Beeler *et al.*[90] showed that the shell method tends to overestimate interstitial formation energies by 10%–15% but gives accurate vacancy formation energies. There may be similar overestimation of migration, binding, and formation energies of the configurations studied here. Unfortunately, using a larger supercell is both impractical and, at least for γ-uranium, impossible: using a $4 \times 4 \times 4$ supercell or larger with the shell method and the interatomic potential of Smirnova *et al.*[91] resulted in unrealistically small or even negative vacancy formation energies (data not shown).

To calculate the migration energy, each initial state was relaxed with respect to internal coordinates and volume. We determined the transition state by way of a nudged elastic band (NEB)[92,93] calculation with a climbing image as implemented in QuantumESPRESSO. We used five images in the NEB calculations, all of which used the same shell method as in the single-point energy calculations. The optimization used the Broyden scheme, which is the default suggested in the documentation. The stopping criterion (path_thr) was a force of 0.1 eV/Å.

IV. RESULTS AND DISCUSSION

A. Vacancy formation and impurity–vacancy binding energies

The formation energy of a single vacancy is calculated using Eq. (4). Our results are compared with previously published DFT calculations and experimental results in Table II. Our results are in good agreement with both previous DFT studies. Xian *et al.*[94] also used 54 atoms in their supercell, but our vacancy formation energy is higher by 0.2 eV. Discrepancies could arise from their use of a $6 \times 6 \times 6$ k-point mesh, whereas we used $5 \times 5 \times 5$. Beeler *et al.*[90] used a supercell of 128 atoms to calculate the vacancy formation energy. The experimental values bracket our results and those of Beeler *et al.*:[90] The earlier work of Matter *et al.*[95] found a formation energy of 1.2 ± 0.3 eV, whereas Lund *et al.*[96] found 1.6 ± 0.2 eV.

We are not aware of any previous reports of calculations of solute–vacancy ($X-\square$) binding energies in γ-uranium; therefore, we calculated these ourselves. We chose solutes so as to compare to diffusion measurements by Rothman and co-workers.[50–52] The results are shown in Table III. All of the solute–vacancy binding energies in γ-uranium are substantially higher than in other bcc metals. For example, in iron and tungsten, the $X-\square$ binding energy varies from −0.6 to 0.6 eV for a variety of solutes.[97–100] In γ-uranium, however, the binding energy varies from 5.715 (Fe$-\square$) to 6.619 eV (Cr$-\square$), which indicates that the solute–vacancy binding energy is much higher in bcc uranium than it is in other bcc metals.

TABLE II. Vacancy formation energy (eV) of γ-uranium compared with previously published results.

Source	Energy (eV)
Present work	1.28
Beeler *et al.*[90]	1.384
Xian *et al.*[94]	1.08
Matter *et al.* (expt.)[95]	1.2 ± 0.3
Lund *et al.* (expt.)[96]	1.6 ± 0.2

TABLE III. Solute–vacancy binding energies in γ-uranium for various solutes near a vacancy. Positive energies indicate energetically favorable binding.

Solute	Binding energy (eV)
Xe	6.034
Mo	6.249
Fe	5.715
Co	5.876
Au	6.450
Cr	6.619
Zr	6.318
Nb	6.113

The solute–vacancy binding energy characterizes the interaction between a solute and a vacancy, which modifies the local concentration of vacancies near a solute. In the case of γ-uranium, the interaction between a solute and a vacancy is strongly attractive. The total solute–vacancy binding energy can be decomposed into two factors: elastic effects and electrostatic effects.[101] The elastic energy (or elastic binding energy) is the energy that is released if the strain fields of a solute and a vacancy interact.[98,100] Due to the unstable nature of γ-uranium at low temperatures, the elastic binding energy contributes significantly to the total solute–vacancy binding energy and may be the primary reason for the high value of the solute–vacancy binding energy in bcc uranium. We are uncertain as to whether the shell method—that is, the frozen layer of atoms near the position of the solute—has any contributions to the binding energy here, but suffice it to say that the values in Table III should be interpreted with caution due to the unstable nature of the uranium bcc lattice arrangement.

It is difficult to envision using a technique such as Born–Oppenheimer molecular dynamics to compute these values at finite temperatures, but that is likely the only way to achieve significant improvements on these values using DFT-based techniques.

B. Xenon and molybdenum diffusion

The process of xenon diffusion is vacancy-assisted in γ-uranium. The net process likely involves diffusion of a vacancy (i.e., uranium self-diffusion) to a position near a particular xenon atom. The xenon atom then exchanges with the vacancy, and the vacancy jumps away by exchanging with other metal atoms. Subsequently, another vacancy encounters the same xenon atom, and it jumps—either back to its original position or to one of the eight other directions, depending on where the vacancy approaches it—by exchanging with the vacancy again. The process repeats in this manner. The result is that xenon diffusion is coupled with uranium self-diffusion (i.e., the diffusion of vacancies). If we assume that only the nearest-neighbor lattice sites matter, then the rate of vacancy exchange with xenon can be estimated by calculating the activation energy associated with xenon exchange with vacancies. We will ignore the possibility of multiple adjacent vacancies, as we expect these to form bubbles (with very low rates of transport) whenever such combinations occur near xenon.

Migration energies are calculated using the climbing-image nudged elastic band method. We calculated the migration energies of xenon and molybdenum moving from the center of the supercell to one of the nearest-neighbor lattice sites. Such solute–vacancy exchange is the primary mechanism of diffusion of xenon and molybdenum because of their size relative to uranium—that is, xenon occupies substitutional positions on the uranium lattice rather than interstitial positions. Table IV presents our findings. Note that in bcc lattices, all eight nearest-neighbor sites are symmetrically equivalent; therefore, there is only one unique migration energy for xenon or molybdenum near seven uranium atoms and one vacancy. The calculated activation energy of a molybdenum jump (in the absence of xenon or other molybdenum atoms), 2.067 eV, is consistent with the observed migration energy of molybdenum in γ-U–Mo at various compositions (2.02–2.08 eV) from the work of Huang *et al.*[102] and slightly higher than the range (1.53–1.91 eV) found in an earlier study by the same investigators.[103] The migration energy of xenon in the absence of molybdenum (0.161 eV) is reasonably close to the (non-rate-limiting) value of 0.11 eV corresponding to the xenon migration energy between cation sites in UO_2 found by Ball and Grimes.[42] As the amount of molybdenum in the nearest-neighbor shell increases, there are more and more symmetrically distinct migration pathways. The migration energy of xenon in the absence of any molybdenum in the nearest-neighbor positions is significantly lower than the migration energy of molybdenum. The Xe−□ binding energy is also lower than the Mo−□ binding energy, which may occur in part because xenon tends to find its energetic minimum location in between the empty lattice site and the site closest to the xenon atom, resulting in shorter jump distances and lower barriers. It should be noted that xenon tends to agglomerate into bubbles[27–31] and that these bubbles would not move by the single-vacancy, single-xenon mechanism assumed here. The net effect is that xenon would move much more slowly once such bubbles form. Xenon transport is also affected by radiation-induced defect formation and localized melting induced by displacement cascades.[104]

TABLE IV. Xenon migration energy (E_m) for different configurations.

Composition[a]	Xe jump	E_m (eV)
7 U	⟨111⟩ [Fig. 1(a)]	0.161
1 Mo	1 [Fig. 1(b)]	0.313
	2 [Fig. 1(b)]	0.172
	3 [Fig. 1(b)]	0.261
2 Mo	1 [Fig. 2(a)]	0.110
	2 [Fig. 2(a)]	0.212
	3 [Fig. 2(b)]	0.532
	4 [Fig. 2(b)]	0.108
	5 [Fig. 2(b)]	0.224
	6 [Fig. 2(c)]	0.110
3 Mo	1 [Fig. 3(a)]	0.515
	2 [Fig. 3(a)]	0.917
	3 [Fig. 3(a)]	0.265
	4 [Fig. 3(a)]	0.579
	5 [Fig. 3(b)]	0.201
	6 [Fig. 3(b)]	0.384
	7 [Fig. 3(b)]	0.386
	8 [Fig. 3(c)]	1.213
	9 [Fig. 3(c)]	0.461
	10 [Fig. 3(c)]	0.435
	Mo jump	E_m (eV)
7 U	⟨111⟩ [Fig. 1(a)]	2.067

[a]The eight nearest-neighbor sites consist of one vacancy plus the atoms listed, with the remaining sites occupied by uranium atoms.

We studied the xenon migration energy in the presence of molybdenum in a systematic way by including various numbers of molybdenum atoms in the nearest-neighbor (NN) shell around a xenon atom and calculating all symmetrically distinct xenon migration energies associated with each distinct arrangement of molybdenum atoms around a central xenon atom. One molybdenum in the NN shell creates three symmetrically equivalent xenon jumps [see Fig. 1(b)]. These three migration pathways (labeled 1, 2, and 3) show higher activation energies than the case with no molybdenum atoms in the NN shell.

In the presence of a vacancy, xenon tends to take a position in between the vacancy and the nearest lattice site at the energy minimum. This results in a very low migration energy for xenon to move to the nearest vacancy. This behavior is very similar to how xenon moves in UO_2 fuel: in UO_2, the xenon atoms prefer to find their lowest-energy location in between the original trap site and the second uranium vacancy.[27] Adding one molybdenum to the nearest-neighbor shell increases the migration energies for all three unique migration pathways. The relative locations of the molybdenum atom and the vacancy change the minimum-energy location of the xenon atom. Xenon tends to relax toward the vacancy and the extra space created by the molybdenum atom. It finds a low-energy site in between its original site, the vacancy, and the molybdenum atom, which increases the migration energy.

There is more than one way to put two molybdenum atoms in the NN shell around a solute atom in a bcc crystal, and three of these arrangements create distinct xenon migration pathways. Figure 2 shows all symmetrically distinct locations for two

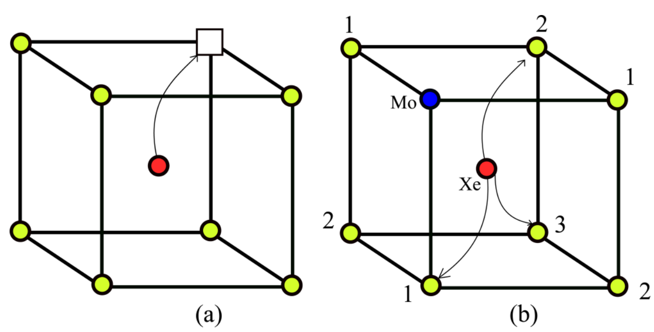

FIG. 1. Diagram of a xenon jump from the center site to a nearest-neighbor vacancy in γ-uranium. (a) All eight possible jumps (initial locations for the vacancy) are symmetrically equivalent with no molybdenum present (only one is shown). (b) With one molybdenum atom in the nearest-neighbor shell, there are three unique initial locations for the vacancy (1, 2, and 3).

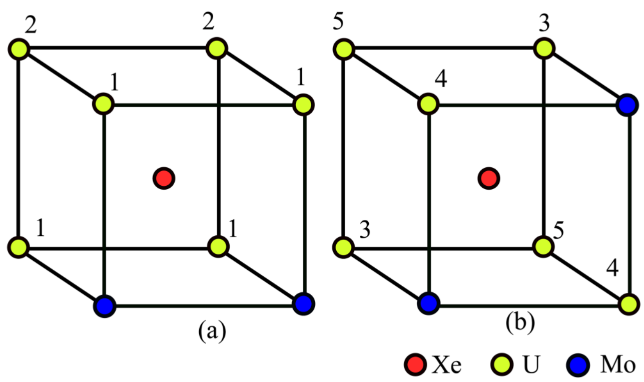

FIG. 2. The three sets of symmetrically inequivalent hops of xenon from the center with two molybdenum atoms in the nearest-neighbor shell with molybdenum atoms initially placed along the same (a) [1 0 0], (b) [1 1 0], and (c) [1 1 1] crystallographic directions. The numbers denote symmetrically distinct locations for the vacancy and correspond to unique migration pathways.

molybdenum atoms around a xenon atom and the resulting symmetrically distinct jumps that could result if a vacancy were in another position nearby. Migration energies with two molybdenum atoms present range from 0.110 to 0.532 eV. Both the positions of the two molybdenum atoms and the direction of the jump influence the migration energy. Directions 1 and 2 [Fig. 2(a)] have migration energies of 0.110 and 0.212 eV, respectively; direction 2 has almost double the migration energy of direction 1. Directions 1, 4, and 6, which all have a molybdenum atom on the corner of the cube adjacent to the vacancy, have the lowest migration energies. The lowest-energy locations for xenon for jumps in directions 1, 4, and 6 are close to each other, which produces a very low migration energy.

Figure 3 shows the symmetrically distinct arrangements of three molybdenum atoms in the nearest-neighbor shell. This local concentration creates ten distinct jumps of a xenon atom to a nearest-neighbor vacancy (Fig. 3). The migration energies for three-molybdenum configurations vary from 0.201 eV for direction 5 to 1.213 eV for direction 8. The highest migration energy is for a xenon atom that jumps to a site between two molybdenum atoms [site 8 in Fig. 3(c)]. Figure 3(a) shows the arrangements of three molybdenum atoms on the same (1 0 0) plane, which produces four distinct jumps with migration energies ranging from 0.515 to 0.917 eV, the highest one being for direction 2, where xenon moves to the opposite corner from the three molybdenum atoms. Figure 3(b) has a combination of two molybdenum atoms on one face of the cell and one molybdenum atom in the lower corner on the opposite site. This configuration reduces the migration energy compared to the configuration in which all three molybdenum atoms are co-planar. Direction 8 [Fig. 3(c)] produces the highest migration energy for xenon. In this configuration, the initial minimum-energy position for xenon is equidistant from all three molybdenum atoms. The final position is not equidistant but creates a larger activation energy. In the cases of directions 9 and 10, the location of the vacancy changes the lowest-energy location (final position) for xenon and reduces the barrier.

We did not calculate the migration energy of xenon with more than three molybdenum atoms in the nearest-neighbor shell. The assumption of a random (binomial) distribution (Table I) implies that the probability of having 0–3 molybdenum atoms near a xenon solute is much higher ($>$ 96%) than having more than three molybdenum atoms for either U-10Mo or U-7Mo.

It should be noted that the use of the "shell" method, in which atoms that are more than approximately 1.5a away from the center of the supercell are held at their crystallographic positions and not allowed to move, creates some uncertainty in the values of all of the migration, binding, and formation energies presented here. The qualitative trends in all of these values (e.g., that xenon migration energies in pure uranium are lower than they are with a single molybdenum atom nearby) are likely to be similar in the absence of such constraints, but the absolute values may not be. It is impossible to perform these calculations in an unconstrained supercell because the γ-uranium lattice is not thermodynamically

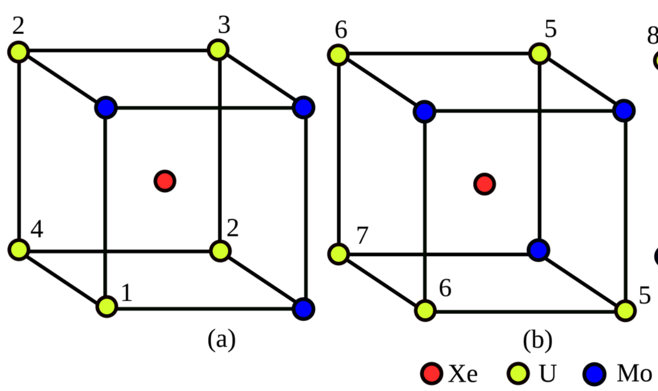

FIG. 3. The three sets of symmetrically distinct hops from the center site with three molybdenum atoms in the nearest-neighbor shell with molybdenum atoms initially placed in the same (a) (1 0 0), (b) (1 1 0), and (c) (1 1 1) crystallographic planes. The numbers denote symmetrically distinct initial locations for the vacancy, each of which creates a unique migration pathway.

stable at low temperatures. This instability results in nonsensical energies for anything larger than an approximately $3 \times 3 \times 3$ "movable" region. The energy values here can be used as benchmarks for interatomic potentials. The only way to use DFT-based methods to improve the uncertainty in these calculations would be to use a time-dependent method, such as Born–Oppenheimer molecular dynamics, as employed by Castellano *et al.*[22]

V. CONCLUSIONS

We calculated solute–vacancy binding energies for different solutes in bcc uranium. Uranium shows relatively high vacancy–solute binding energies compared to iron and aluminum. The unstable nature of γ-uranium at low temperature contributes to a significant increase in solute–vacancy binding energy relative to other bcc metals. The higher elastic binding energy in bcc uranium produces a high solute–vacancy binding energy.

We also calculated migration energies of xenon and molybdenum in pure bcc uranium. Molybdenum's migration energy is very high compared to that of xenon, indicating that in pure bcc uranium, xenon moves much faster than molybdenum. The relatively low diffusivity of molybdenum also supports our assumption that molybdenum is randomly distributed in uranium–molybdenum alloys (presuming that the manufacturing process initially starts with a melt or powder that produces an ideal mixture). We also studied migration energies of xenon in the presence of molybdenum in U–Mo alloys. Different arrangements of molybdenum atoms in the nearest-neighbor shell and the distinct jumps available to xenon are identified and their activation energies are calculated. The binomial distribution suggests that having up to three molybdenum atoms in the nearest-neighbor shell is highly probable in U-10Mo and U-7Mo alloys. The presence of molybdenum in the nearest-neighbor shell of a xenon atom has an impact on the migration energy, but it does not generally increase or decrease the migration energy; both the locations of the molybdenum atoms and the direction of the jump influence the migration energy. Having one molybdenum atom in the nearest-neighbor shell increases the activation energy between 0.01 and 0.15 eV, depending on the location of the molybdenum atom relative to the xenon atom and the vacancy. If xenon has two molybdenum atoms nearby, we found a similar increase, though there are combinations for which the migration energy is lower than it is in the single-molybdenum cases. For xenon with three nearby molybdenum atoms, the migration energy increases for all molybdenum/vacancy arrangements. While there are several molybdenum arrangements that result in decreased migration energies relative to some of the two-molybdenum configurations, the general trend with the addition of molybdenum in the nearest-neighbor shell near xenon is to increase the migration energy, hence reducing xenon mobility in U–Mo alloys. It should be noted that the activation energies of most xenon jumps found here are as low or lower than the calculated activation energies for uranium self-diffusion, which are in the 0.5–1 eV range as calculated with embedded atom method interatomic potentials.[57,58,105] This suggests that the rate-limiting process in xenon diffusion may be uranium self-diffusion (excluding the possibility of divacancy formation near xenon).

We did not consider the influence of molybdenum in the second-nearest-neighbor shell in bcc uranium. Future work should include a determination of the effective diffusion coefficient of xenon in U–Mo alloys using the kinetic Monte Carlo method. Future work should also explore the free energy landscape at finite temperature through techniques such as Born–Oppenheimer molecular dynamics. Such techniques might address the questions present here regarding whether the "shell" approximation is adequate to model xenon diffusion in γ-uranium.

SUPPLEMENTARY MATERIAL

See the supplementary material for the atomic coordinates of the solute–vacancy binding energy calculations in Table III.

ACKNOWLEDGMENTS

A.R.M.I. is grateful for helpful discussions with Amir Mofrad (MU). Partial financial support for this work was provided by the U.S. Nuclear Regulatory Commission under Award No. NRC-HQ-84-15-G-0026. A portion of the computation for this work was performed on the high-performance computing infrastructure provided in part by Research Computing Support Services and in part by the National Science Foundation under Grant No. CNS-1429294 at the University of Missouri. This research also used computational resources of the National Energy Research Scientific Computing Center (NERSC), a U.S. Department of Energy Office of Science User Facility at Lawrence Berkeley National Laboratory, operated under Contract No. DE-AC02-05CH11231.

AUTHOR DECLARATIONS

Conflict of Interest

The authors have no conflicts to disclose.

DATA AVAILABILITY

The data that support the findings of this study are available within the article. Atomic configurations corresponding to the data in Table III are available as supplementary material. Atomic coordinates corresponding to the initial, final, and transition states in Table IV are available from the authors upon reasonable request.

REFERENCES

[1] J. L. Snelgrove, G. L. Hofman, M. K. Meyer, C. L. Trybus, and T. C. Wiencek, "Development of very-high-density low-enriched-uranium fuels," Nucl. Eng. Des. **178**, 119–126 (1997).

[2] A. C. Lawson, C. E. Olsen, J. W. Richardson, M. H. Mueller, and G. H. Lander, "Structure of β-uranium," Acta Crystallogr. B **44**, 89–96 (1988).

[3] J. Akella, S. Weir, J. M. Wills, and P. Söderlind, "Structural stability in uranium," J. Phys. Condens. Matter **9**, L549–L555 (1997).

[4] J. H. Kittel, B. R. T. Frost, J. P. Mustelier, K. Q. Bagley, G. C. Crittenden, and J. Van Dievoet, "History of fast reactor fuel development," J. Nucl. Mater. **204**, 1–13 (1993).

[5] A. S. Wilson and R. E. Rundle, "The structures of uranium metal," Acta Crystallogr. **2**, 126–127 (1949).

[6] V. P. Sinha, P. V. Hegde, G. J. Prasad, G. K. Dey, and H. S. Kamath, "Phase transformation of metastable cubic γ-phase in U–Mo alloys," J. Alloys Compd. **506**, 253–262 (2010).

[7]H. L. Yakel, "Crystal structures of transition phases formed in U/16.60 at% Nb/5.64 at% Zr alloys," J. Nucl. Mater. **33**, 286–295 (1969).
[8]V. P. Sinha, P. V. Hegde, G. J. Prasad, G. K. Dey, and H. S. Kamath, "Effect of molybdenum addition on metastability of cubic γ-uranium," J. Alloys Compd. **491**, 753–760 (2010).
[9]N.-T. H. Kim-Ngan and L. Havela, "Superconductivity in U-T alloys (T = Mo, Pt, Pd, Nb, Zr) stabilized in the cubic γ-U structure by splat-cooling technique," J. Sci. Adv. Mater. Dev. **1**, 121–127 (2016).
[10]"Mo (molybdenum) binary alloy phase diagrams," in *Alloy Phase Diagrams*, ASM Handbook Vol. 3, edited by H. Okamoto, M. E. Schlesinger, and E. M. Mueller (ASM International, 2016), pp. 489–498.
[11]A. Berche, N. Dupin, C. Guénau, C. Rado, B. Sundman, and J. C. Dumas, "Calphad thermodynamic description of some binary systems involving U," J. Nucl. Mater. **411**, 131–143 (2011).
[12]R. Prabhakaran, "U-Mo monolithic fuel for nuclear research and test reactors," JOM **69**, 2529–2531 (2017).
[13]M. K. Meyer, J. Gan, J. F. Jue, D. D. Keiser, E. Perez, A. Robinson, D. M. Wachs, N. Woolstenhulme, G. L. Hofman, and Y. S. Kim, "Irradiation performance of U-Mo monolithic fuel," Nucl. Eng. Technol. **46**, 169–182 (2014).
[14]W. Williams, A. Robinson, and B. Rabin, "Post-irradiation non-destructive analyses of the AFIP-7 experiment," JOM **69**, 2546–2553 (2017).
[15]A. E. Dwight, "The uranium-molybdenum equilibrium diagram below 900 C," J. Nucl. Mater. **2**, 81–87 (1960).
[16]K. Tangri and G. Williams, "Metastable phases in the uranium molybdenum system and their origin," J. Nucl. Mater. **4**, 226–233 (1961).
[17]A. Berche, N. Dupin, C. Guéneau, C. Rado, B. Sundman, and J. C. Dumas, "Calphad thermodynamic description of some binary systems involving U," J. Nucl. Mater. **411**, 131–143 (2011).
[18]X. Zhang, Y. F. Cui, G. L. Xu, W. J. Zhu, H. S. Liu, B. Y. Yin, and Z. P. Jin, "Thermodynamic assessment of the U–Mo–Al system," J. Nucl. Mater. **402**, 15–24 (2010).
[19]E. L. Losada and J. E. Garcés, "On the ground state of the U-Mo system," J. Nucl. Mater. **518**, 380–385 (2019).
[20]A. Landa, P. Söderlind, and P. E. A. Turchi, "Density-functional study of U–Mo and U–Zr alloys," J. Nucl. Mater. **414**, 132–137 (2011).
[21]P. R. Alonso and G. H. Rubiolo, "The role of multisite interactions in the formation energy of bcc γ (U, Mo) disordered phase," Model. Simulat. Mater. Sci. Eng. **15**, 263 (2007).
[22]A. Castellano, F. Bottin, B. Dorado, and J. Bouchet, "Thermodynamic stabilization of γ-U–Mo alloys: Effect of Mo content and temperature," Phys. Rev. B **101**, 184111 (2020).
[23]V. V. Rondinella and T. Wiss, "The high burn-up structure in nuclear fuel," Mater. Today **13**, 24–32 (2010).
[24]A. R. M. Iasir, N. J. Peters, and K. D. Hammond, "Estimation of effective thermal conductivity in U-10Mo fuels with distributed xenon gas bubbles," J. Nucl. Mater. **508**, 159–167 (2018).
[25]J. Rest, Y. S. Kim, G. L. Hofman, M. K. Meyer, and S. L. Hayes, "U–Mo fuels handbook," version 1.0, Technical Report ANL-09/31, Argonne National Laboratory, Argonne, IL, 2006.
[26]R. W. Grimes and C. R. A. Catlow, "The stability of fission products in uranium dioxide," Philos. Trans. R. Soc., A **335**, 609–634 (1991).
[27]D. A. Andersson, B. P. Uberuaga, P. V. Nerikar, C. Unal, and C. R. Stanek, "U and Xe transport in $UO_2 \pm x$: Density functional theory calculations," Phys. Rev. B **84**, 054105 (2011).
[28]B. D. Miller, J. Gan, J. Madden, J.-F. Jue, A. Robinson, and D. D. Keiser, "Advantages and disadvantages of using a focused ion beam to prepare TEM samples from irradiated U–10Mo monolithic nuclear fuel," J. Nucl. Mater. **424**, 38–42 (2012).
[29]B. D. Miller, J. Gan, D. D. Keiser, Jr., A. B. Robinson, J. F. Jue, J. W. Madden, and P. G. Medvedev, "Transmission electron microscopy characterization of the fission gas bubble superlattice in irradiated U–7wt% Mo dispersion fuels," J. Nucl. Mater. **458**, 115–121 (2015).
[30]J. Gan, D. D. Keiser, D. M. Wachs, A. B. Robinson, B. D. Miller, and T. R. Allen, "Transmission electron microscopy characterization of irradiated U–7Mo/Al–2Si dispersion fuel," J. Nucl. Mater. **396**, 234–239 (2010).
[31]J. Gan, D. D. Keiser, B. D. Miller, A. B. Robinson, J.-F. Jue, P. Medvedev, and D. M. Wachs, "TEM characterization of U–7Mo/Al–2Si dispersion fuel irradiated to intermediate and high fission densities," J. Nucl. Mater. **424**, 43–50 (2012).
[32]S. Van den Berghe, W. Van Renterghem, and A. Leenaers, "Transmission electron microscopy investigation of irradiated U–7wt% Mo dispersion fuel," J. Nucl. Mater. **375**, 340–346 (2008).
[33]S. Hu, W. Setyawan, V. V. Joshi, and C. A. Lavender, "Atomistic simulations of thermodynamic properties of Xe gas bubbles in U10Mo fuels," J. Nucl. Mater. **490**, 49–58 (2017).
[34]Y. Yun, H. Kim, H. Kim, and K. Park, "Atomic diffusion mechanism of Xe in UO_2," J. Nucl. Mater. **378**, 40–44 (2008).
[35]J. C. Carter, E. J. Driscoll, and T. S. Elleman, "Xenon-133 diffusion and trapping in single-crystal uranium dioxide," Phys. Status Solidi A **14**, 673–680 (1972).
[36]H. Matzke, "Diffusion in doped UO_2," Nucl. Appl. **2**, 131–137 (1966).
[37]J. R. MacEwan and W. H. Stevens, "Xenon diffusion in UO_2: Some complicating factors," J. Nucl. Mater. **11**, 77–93 (1964).
[38]K. Une, I. Tanabe, and M. Oguma, "Effects of additives and the oxygen potential on the fission gas diffusion in UO_2 fuel," J. Nucl. Mater. **150**, 93–99 (1987).
[39]C. R. A. Catlow, "Fission gas diffusion in uranium dioxide," Proc. R. Soc. A **364**, 473–497 (1978).
[40]R. A. Jackson, A. D. Murray, J. H. Harding, and C. R. A. Catlow, "The calculation of defect parameters in UO_2," Philos. Mag. A **53**, 27–50 (1986).
[41]R. W. Grimes, C. R. A. Catlow, and A. M. Stoneham, "Calculations of solution energies of fission products in uranium dioxide," J. Am. Ceram. Soc. **72**, 1856–1860 (1989).
[42]R. G. J. Ball and R. W. Grimes, "Diffusion of Xe in UO_2," J. Chem. Soc. Faraday Trans. **86**, 1257–1261 (1990).
[43]T. Petit, G. Jomard, C. Lemaignan, B. Bigot, and A. Pasturel, "Location of krypton atoms in uranium dioxide," J. Nucl. Mater. **275**, 119–123 (1999).
[44]J.-P. Crocombette, "*Ab initio* energetics of some fission products (Kr, I, Cs, Sr and He) in uranium dioxide," J. Nucl. Mater. **305**, 29–36 (2002).
[45]M. Freyss, N. Vergnet, and T. Petit, "*Ab initio* modeling of the behavior of helium and xenon in actinide dioxide nuclear fuels," J. Nucl. Mater. **352**, 144–150 (2006).
[46]G. Neumann and C. Tuijn, *Self-Diffusion and Impurity Diffusion in Pure Metals: Handbook of Experimental Data* (Elsevier, 2008), Chap. 10, pp. 333–348.
[47]A. Paul and S. Divinski, *Handbook of Solid State Diffusion: Volume 2: Diffusion Analysis in Material Applications* (Elsevier, 2017), Chap. 8, pp. 339–372.
[48]H. Matzke, "Diffusion processes in nuclear fuels," in *Diffusion Processes in Nuclear Materials*, edited by R. P. Agarwala (North-Holland, 1992), pp. 9–69.
[49]Y. Adda and A. Kirianenko, "Etude de l'autodiffusion de l'uranium en phase γ," J. Nucl. Mater. **1**, 120–126 (1959).
[50]N. L. Peterson and S. J. Rothman, "Diffusion in gamma uranium," Phys. Rev. **136**, A842 (1964).
[51]S. J. Rothman, L. T. Lloyd, R. Weil, and A. L. Harkness, "Self-diffusion in gamma uranium," Technical Report ANL-5971, Argonne National Laboratory, Lemont, IL, 1959.
[52]S. J. Rothman, "The diffusion of gold in gamma uranium," J. Nucl. Mater. **3**, 77–80 (1961).
[53]Y. Adda and A. Kirianenko, "Etude de l'autodiffusion de l'uranium en phase α," J. Nucl. Mater. **6**, 130–134 (1962).
[54]R. Resnick and L. L. Seigle, "The self-diffusion of alpha-uranium," J. Nucl. Mater. **5**, 5–11 (1962).
[55]S. J. Rothman, J. Gray, Jr., J. P. Hughes, and A. L. Harkness, "Self-diffusion in beta uranium," J. Nucl. Mater. **3**, 72–76 (1961).

[56]Y. Liu, D. Yu, Y. Du, G. Sheng, Z. Long, J. Wang, and L. Zhang, "Atomic mobilities, diffusivities and their kinetic implications for U–X (X = Ti, Nb and Mo) bcc alloys," Calphad **37**, 49–56 (2012).
[57]D. E. Smirnova, A. Y. Kuksin, S. V. Starikov, and V. V. Stegailov, "Atomistic modeling of the self-diffusion in γ-U and γ-U-Mo," Phys. Met. Metallogr. **116**, 445–455 (2015).
[58]D. E. Smirnova, A. Y. Kuksin, and S. V. Starikov, "Investigation of point defects diffusion in bcc uranium and U–Mo alloys," J. Nucl. Mater. **458**, 304–311 (2015).
[59]J. B. Adams, S. M. Foiles, and W. G. Wolfer, "Self-diffusion and impurity diffusion of fcc metals using the five-frequency model and the embedded atom method," J. Mater. Res. **4**, 102–112 (1989).
[60]P. E. Blöchl, E. Smargiassi, R. Car, D. B. Laks, W. Andreoni, and S. T. Pantelides, "First-principles calculations of self-diffusion constants in silicon," Phys. Rev. Lett. **70**, 2435 (1993).
[61]P. E. Blöchl, C. G. Van de Walle, and S. T. Pantelides, "First-principles calculations of diffusion coefficients: Hydrogen in silicon," Phys. Rev. Lett. **64**, 1401 (1990).
[62]W. Frank, U. Breier, C. Elsässer, and M. Fähnle, "First-principles calculations of absolute concentrations and self-diffusion constants of vacancies in lithium," Phys. Rev. Lett. **77**, 518 (1996).
[63]A. Janotti, M. Krčmar, C. L. Fu, and R. C. Reed, "Solute diffusion in metals: Larger atoms can move faster," Phys. Rev. Lett. **92**, 085901 (2004).
[64]M. Krčmar, C. L. Fu, A. Janotti, and R. C. Reed, "Diffusion rates of 3D transition metal solutes in nickel by first-principles calculations," Acta Mater. **53**, 2369–2376 (2005).
[65]V. Milman, M. C. Payne, V. Heine, R. J. Needs, J. S. Lin, and M. H. Lee, "Free energy and entropy of diffusion by *ab initio* molecular dynamics: Alkali ions in silicon," Phys. Rev. Lett. **70**, 2928 (1993).
[66]N. Sandberg, B. Magyari-Köpe, and T. R. Mattsson, "Self-diffusion rates in Al from combined first-principles and model-potential calculations," Phys. Rev. Lett. **89**, 065901 (2002).
[67]A. B. Lidiard, "CXXXIII. Impurity diffusion in crystals (mainly ionic crystals with the sodium chloride structure)," Philos. Mag. Series 7 **46**, 1218–1237 (1955).
[68]A. B. Lidiard, "The influence of solutes on self-diffusion in metals," Philos. Mag. A **5**, 1171–1180 (1960).
[69]A. D. Leclaire and A. B. Lidiard, "LIII. Correlation effects in diffusion in crystals," Philos. Mag. A **1**, 518–527 (1956).
[70]A. D. Le Claire, "Solvent self-diffusion in dilute b.c.c. solid solutions," Philos. Mag. A **21**, 819–832 (1970).
[71]H. Mehrer, *Diffusion in Solids: Fundamentals, Methods, Materials, Diffusion-Controlled Processes* (Springer Science & Business Media, 2007), Vol. 155, pp. 116–122.
[72]G. H. Vineyard and G. J. Dienes, "The theory of defect concentration in crystals," Phys. Rev. **93**, 265–268 (1954).
[73]G. H. Vineyard, "Frequency factors and isotope effects in solid state rate processes," J. Phys. Chem. Solids **3**, 121–127 (1957).
[74]H. Eyring, "The activated complex in chemical reactions," J. Chem. Phys. **3**, 107–115 (1935).
[75]M. G. Evans and M. Polanyi, "Some applications of the transition state method to the calculation of reaction velocities, especially in solution," Trans. Faraday Soc. **31**, 875–894 (1935).
[76]K. Heinola and T. Ahlgren, "Diffusion of hydrogen in bcc tungsten studied with first principle calculations," J. Appl. Phys. **107**, 113531 (2010).
[77]B. Beeler, S. Hu, Y. Zhang, and Y. Gao, "A improved equation of state for Xe gas bubbles in γ U-Mo fuels," J. Nucl. Mater. **530**, 151961 (2020).
[78]R. W. Balluffi and P. S. Ho, *Diffusion* (American Society for Metals, Metals Park, Ohio, 1973), p. 83.
[79]C. Wolverton, "Solute–vacancy binding in aluminum," Acta Mater. **55**, 5867–5872 (2007).
[80]P. Giannozzi, S. Baroni, N. Bonini, M. Calandra, R. Car, C. Cavazzoni, D. Ceresoli, G. L. Chiarotti, M. Cococcioni, I. Dabo, A. Dal Corso, S. de Gironcoli, S. Fabris, G. Fratesi, R. Gebauer, U. Gerstmann, C. Gougoussis, A. Kokalj, M. Lazzeri, L. Martin-Samos, N. Marzari, F. Mauri, R. Mazzarello, S. Paolini, A. Pasquarello, L. Paulatto, C. Sbraccia, S. Scandolo, G. Sclauzero, A. P. Seitsonen, A. Smogunov, P. Umari, and R. M. Wentzcovitch, "QUANTUM ESPRESSO: A modular and open-source software project for quantum simulations of materials," J. Phys. Condens. Matter **21**, 395502 (2009).
[81]P. E. Blöchl, "Projector augmented-wave method," Phys. Rev. B **50**, 17953–17979 (1994).
[82]A. R. M. Iasir and K. D. Hammond, "Pseudopotential for plane-wave density functional theory studies of metallic uranium," Comput. Mater. Sci. **171**, 109221 (2020).
[83]Quantum ESPRESSO, "PSlibrary"; see http://www.quantum-espresso.org/pseudopotentials (2019).
[84]A. Dal Corso, "Pseudopotentials periodic table: From H to Pu," Comput. Mater. Sci. **95**, 337–350 (2014).
[85]J. P. Perdew, K. Burke, and M. Ernzerhof, "Generalized gradient approximation made simple," Phys. Rev. Lett. **77**, 3865–3868 (1996).
[86]J. P. Perdew, K. Burke, and M. Ernzerhof, "Generalized gradient approximation made simple (Errata)," Phys. Rev. Lett. **78**, 1396 (1997).
[87]P. Söderlind, "Theory of the crystal structures of cerium and the light actinides," Adv. Phys. **47**, 959–998 (1998).
[88]Y.-Y. Ye, Y. Chen, K.-M. Ho, B. N. Harmon, and P.-A. Lindgård, "Phonon-phonon coupling and the stability of the high-temperature bcc phase of Zr," Phys. Rev. Lett. **58**, 1769–1772 (1987).
[89]J. M. Sanchez and D. De Fontaine, "Model for anomalous self-diffusion in group-IV B transition metals," Phys. Rev. Lett. **35**, 227–230 (1975).
[90]B. Beeler, B. Good, S. Rashkeev, C. Deo, M. Baskes, and M. Okuniewski, "First principles calculations for defects in U," J. Phys. Condens. Matter **22**, 505703 (2010).
[91]D. E. Smirnova, A. Y. Kuksin, S. V. Starikov, V. V. Stegailov, Z. Insepov, J. Rest, and A. M. Yacout, "A ternary EAM interatomic potential for U–Mo alloys with Xenon," Model. Simulat. Mater. Sci. Eng. **21**, 035011 (2013).
[92]G. Henkelman, B. P. Uberuaga, and H. Jónsson, "A climbing image nudged elastic band method for finding saddle points and minimum energy paths," J. Chem. Phys. **113**, 9901–9904 (2000).
[93]G. Henkelman and H. Jónsson, "Improved tangent estimate in the nudged elastic band method for finding minimum energy paths and saddle points," J. Chem. Phys. **113**, 9978–9985 (2000).
[94]S. Xiang, H. Huang, and L. Hsiung, "Quantum mechanical calculations of uranium phases and niobium defects in γ-uranium," J. Nucl. Mater. **375**, 113–119 (2008).
[95]H. Matter, J. Winter, and W. Triftshäuser, "Investigation of vacancy formation and phase transformations in uranium by positron annihilation," J. Nucl. Mater. **88**, 273–278 (1980).
[96]K. R. Lund, K. G. Lynn, M. H. Weber, and M. A. Okuniewski, "Vacancy formation enthalpy in polycrystalline depleted uranium," J. Phys. Conf. Ser. **443**, 012021 (2013).
[97]P. Olsson, T. P. C. Klaver, and C. Domain, "*Ab initio* study of solute transition-metal interactions with point defects in bcc fe," Phys. Rev. B **81**, 054102 (2010).
[98]T. Ohnuma, N. Soneda, and M. Iwasawa, "First-principles calculations of vacancy–solute element interactions in body-centered cubic iron," Acta Mater. **57**, 5947–5955 (2009).
[99]E. Vincent, C. Becquart, and C. Domain, "*Ab initio* calculations of vacancy interactions with solute atoms in bcc fe," Nucl. Instrum. Methods Phys. Res. B **228**, 137–141 (2005).
[100]X.-S. Kong, X. Wu, Y.-W. You, C. Liu, Q. Fang, J.-L. Chen, G.-N. Luo, and Z. Wang, "First-principles calculations of transition metal–solute interactions with point defects in tungsten," Acta Mater. **66**, 172–183 (2014).
[101]J. Burke, "The measurement of solute-vacancy interaction energies," J. Less Common Met. **28**, 441–456 (1972).
[102]K. Huang, C. C. Kammerer, D. D. Keiser, Jr., and Y. H. Sohn, "Diffusion barrier selection from refractory metals (Zr, Mo and Nb) via interdiffusion

investigation for U-Mo RERTR fuel alloy," J. Ph. Equilibria Diffus. **35**, 146–156 (2014).
[103]K. Huang, D. D. Keiser, Jr., and Y. Sohn, "Interdiffusion, intrinsic diffusion, atomic mobility, and vacancy wind effect in γ (bcc) uranium-molybdenum alloy," Metall. Mater. Trans. A **44**, 738–746 (2013).
[104]B. Beeler, M. W. D. Cooper, Z.-G. Mei, D. Schwen, and Y. Zhang, "Radiation driven diffusion in γ U-Mo," J. Nucl. Mater. **543**, 152568 (2021).
[105]G. Park, B. Beeler, and M. A. Okuiewski, "An atomistic study of defect energetics and diffusion with respect to composition and temperature in γ U and γ U-Mo alloys," J. Nucl. Mater. **552**, 152970 (2021).